

NEAR-INFRARED OPTICAL COHERENCE TOMOGRAPHY FOR THE INSPECTION OF FIBER COMPOSITES

Ping LIU¹, Liaojun YAO², Roger GROVES¹

¹ Aerospace Non-Destructive Testing Laboratory, Faculty of Aerospace Engineering, Delft University of Technology, Kluyverweg 1, 2600 GB, Delft, The Netherlands;
ping.liu@tudelft.nl

² Structural Integrity & Composites Group, Faculty of Aerospace Engineering, Delft University of Technology, Kluyverweg 1, 2600 GB, Delft, The Netherlands

Abstract. Optical coherence tomography (OCT) is a non-invasive imaging method, which allows the reconstruction of three dimensional depth-resolved images with microscale resolution. Originally developed for biomedical diagnostics, nowadays it also shows a high potential for applications in the field of non-destructive testing (NDT). This work demonstrates how OCT could help to investigate the delamination growth in fiber composites. A customized OCT system was built with a near-infrared light source with center wavelength at 1550 nm. It was used as an inline NDT tool to monitor the crack tips and image the crack surfaces within a glass fiber composite under static loading. For carbon fiber composites, although it is difficult to acquire the internal structures due to their opaque property, OCT can still work as a surface profilometer to reconstruct 3D crack surface profiles, providing substantial information for the study of crack growth in the composites.

1. Introduction

Introducing a reinforcing fiber (e.g. glass fiber and carbon fiber) within a polymer matrix leads to composite materials with improved mechanical properties, e.g. high strength and stiffness to weight ratio. These advantages of composites attract widespread applications, especially in aerospace and wind energy industries. However, this growing market also brings the challenge to determine the structural integrity due to the new forms of defects in composites, such as porosity, cracks, debonding, fiber breakage and delamination [1]. Amongst these defects delamination is probably the most severe damage. The strength and stiffness of composite structures are reduced due to delamination, potentially leading to structural failure.

To investigate the delamination behaviour under tensile loading, usually static or fatigue loadings are performed on double cantilever beam (DCB) specimens which have initial cracks between two middle layers. The delamination growth is recorded by a camera from the side of DCB specimen and the crack lengths are determined based on the crack lines shown in the pictures. After the test, the specimens are split along the delamination cracks and the crack surfaces are further investigated under a microscope [2]. However, it is noticed that these typical tests have several shortcomings in, e.g. determining crack lengths

accurately and providing 3D crack surface profiles, which are of great importance in the delamination research.

Optical Coherence Tomography (OCT) [3] is a microstructural imaging technique based on low coherence interferometry which measures backreflected light from interfaces within a turbid media. Compared with its counterparts such as ultrasonic testing and X-ray computed tomography (X-ray CT), OCT has advantages in: i) no coupling agent is required; ii) no special safety precautions have to be taken; iii) portable size and flexible probe which can be easily adapted to inline inspection. These facts have rendered OCT a favorable non-invasive tool which developed rapidly in the past two decades. Since it was invented in the early 90's for the imaging of the human retina [4], nowadays OCT is not only extensively used in the field of biomedical diagnostics, but it also shows a high potential in the NDT field for material characterization, summarized in [5-7].

This paper demonstrates a customized OCT system for 3D imaging of delamination cracks in composites. OCT was used as an inline inspection tool for monitoring the delamination growth inside a glass fiber composite. It also performed as a surface profilometer to reconstruct 3D crack surfaces from carbon fiber composites.

2. OCT Principles

Generally OCT can be performed in either time domain (TD-OCT) or Fourier domain (FD-OCT). A typical TD-OCT is based on the Michelson interferometer, as shown in Fig. 1(a). low-coherence light from the source is divided by a beamsplitter into reference and sample beams. The beam reflected from the reference mirror is recombined with the sample beam at the same beamsplitter, and finally the interference signal is collected by a photo detector. Due to the broadband nature of the light, interference only can be observed when optical path lengths of the reference and sample arms are matched to within the coherence length of the light. Therefore by translating the reference mirror, a set of interferometric signals will be detected as a function of the reference mirror position. This set corresponds to the axial distribution of scattering interfaces within the specimen and is referred to as an A-scan. By laterally scanning the sample beam in either one or two orthogonal directions, a cross-sectional or volumetric image can be finally obtained.

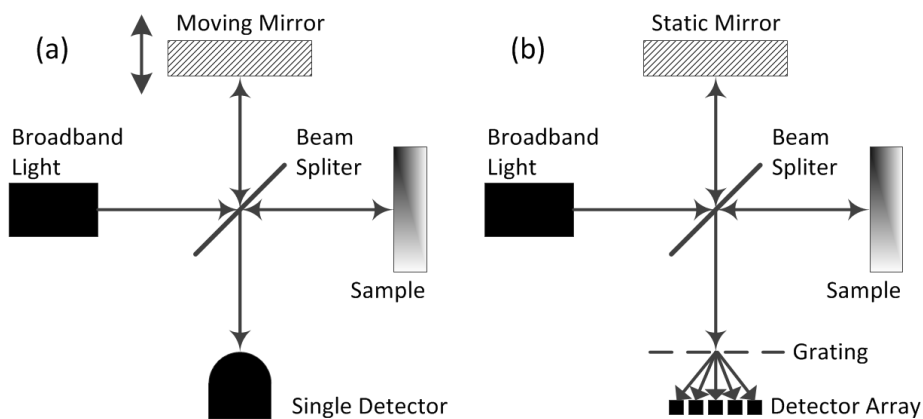


Fig.1. Schematics of (a) TD-OCT system using a moveable reference mirror based on a Michelson interferometer and (b) FD-OCT system by detecting spectrum components with a diffraction grating and a linear detector array.

In FD-OCT, as depicted in Fig. 1(b), the single light intensity detector is replaced by a spectrometer comprising a diffraction grating and a linear CCD detector array. These CCD detectors collect the spectrum of the light source modulated by frequencies of interference fringes, which correspond to positions of scattering layers in a specimen: the deeper the layer is, the higher the modulation frequency will be. Therefore, FD-OCT is able to acquire the entire axial profile of a specimen in one shot in the frequency domain and subsequently to recover this information by reverse Fourier transformation. As no movement of the reference mirror is needed, FD-OCT is much faster than TD-OCT and is only limited by the integration time of CCD detectors [8]. However, the main disadvantage of FD-OCT is the short depth detection range due to the limited number of CCD pixels [9]. The quantitative performance comparison of TD-OCT and FD-OCT is discussed in the next section, by taking a customized OCT system as an example.

3. Instrumentation

In TU Delft, a compact and robust fiber-optic OCT system was built for polymer-based material characterization [10]. A key feature of the instrument is that it integrates TD-OCT and FD-OCT into one system so the individual strengths of each design can give an advantage to different applications. Fig. 2 shows a schematic of the developed OCT system. The light beam from a superluminescent diode (SLD, FESL-1550-20-BTF, Frankfurt Laser Company, Germany), passes through a circulator and is linearly polarized by an optical polarizer. It is then divided by a fiber coupler into reference and sample arms with equal optical power. In the reference arm, light travels through an optical delay line (ODL-650-MC, OZ Optics Ltd, Canada) and arrives in front of a reflector, where it is reflected back along the same path to the fiber coupler. In the sample arm, light passing through a second polarizer is collimated by a collimation lens and then focused to the specimen by an achromatic doublet lens. It is then reflected from the sample and travels back to the same fiber coupler, where it is combined with backreflected reference light and is split again. Half of the light goes back to the circulator and is directed to one input of the balanced detector (PDB420C, Thorlabs GmbH, Germany). Another half goes to an optical switch, which based on the testing request could either direct the recombined light to the second input of the balanced detector for time-domain measurement or feed the light into a spectrometer (NIRQuest512, Ocean Optics Inc, US) for Fourier-domain measurement. Between each axial scan, a pair of orthogonal translation stages (T-LS28M, Zaber Inc, Canada) is utilized to shift the probe beam laterally. The sampling data is stored in a PC and processed to rebuild structural images of the specimen.

The SLD has a center wavelength of 1550 nm, which is less scattering and gives deeper penetration in polymer-based material than the shorter wavelength used for biomedical applications [11]. The light source has a FWHM (Full Width at Half Maximum) of 60 nm, which can provide a theoretical axial resolution [12] of 17 μm in the air, and 11 μm in polymer materials with a 1.55 average refractive index taken into account. The lateral resolution, decided by the beam size in specimens, is 20 μm .

In TD-OCT, The axial scan of TD-OCT in our system is achieved by electrical control of an optical delay line (ODL-650-MC, OZ Optics Ltd, Canada) in the reference arm. The servo motor in the ODL provides a linear resolution of less than 1 μm and can sweep the optical pathlength at a speed of 1.7 mm/s with a maximum of 50 mm range. In FD-OCT, the spectrometer has a minimum of 1 ms integration time and hence reaches 1000 A-scans/s, which is much faster than TD-OCT. However, the spectrometer is configured with a 160 nm spectral range and 512 detector elements, resulting in only 1 mm axial scan range in polymer-based materials. Therefore with this hybrid system, FD-OCT is typically used for fast scan of thin films, e.g. polymer coatings as described in our previous paper [13], while

TD-OCT is ideal for the characterization of thicker materials, e.g. composite laminates as demonstrated in the following section.

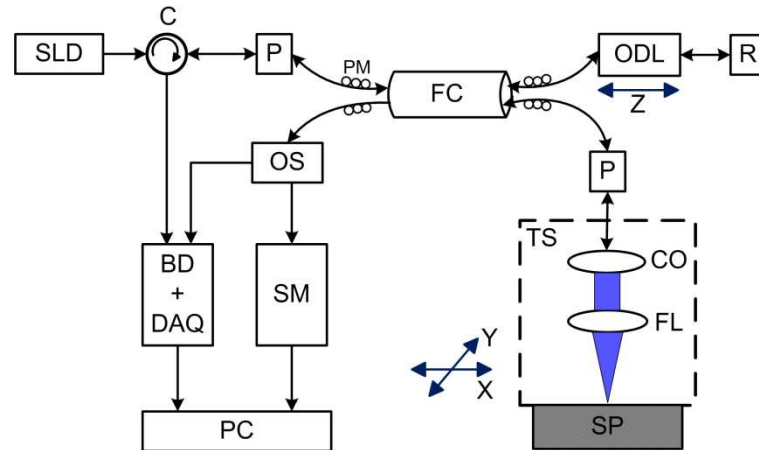


Fig. 2. Schematic setup of a hybrid TD-FD-OCT. Abbreviations: SLD, superluminescent diode; C, Circulator; P, polarizer; PM, polarization maintaining optical fibers; FC, fiber coupler; ODL, optical delay line; R, reflector; CO, collimator; FL, Focusing Lens; TS, translation stage; SP, sample; OS, optical switch; BD, balanced detector; DAQ, data acquisition board; SM, spectrometer; PC, personal computer. X and Y are the two orthogonal lateral directions indicating the movement of the translation stages, and Z is the axial direction indicating the movement of ODL.

4. Results and Discussion

4.1 Glass Fiber Composites

The material tested was a non-crimp glass-fiber epoxy mixture which is generally used for the spar webs in wind turbine blades [14]. A total of 16 layers of glass fiber were used. The fiber orientation of each layer was $+45^\circ$ and -45° , relative to the length direction of the laminate, symmetrically distributed from the middle ($[(\pm 45^\circ)_8 / (\mp 45^\circ)_8]$). To initiate the delamination a non-adhesive Kapton film was placed between two middle layers during the lay-up process. After manufacture, the composite material was cut to form DBC specimens, each of which is approximately 220 mm length, 25 mm width, and 4.4 mm thick. These specimens were then adhesively bonded to a pair of aluminium blocks for tensile loading introduction. The OCT probe was then put in front of the specimen as an inline inspection tool to monitor the delamination growth.

Fig. 3(a) shows a cross-sectional OCT profile of the delamination crack. The first bright line (labeled 1) indicates the location of the front surface of the specimen which was tilted by a small angle to resist strong specular reflections. Below the surface ellipses with lighter contrast are resolved, revealing the distribution of the fiber tows from each layer. At the lower layer of the structure, around 2.2~2.7 mm, an evident feature is posed. Two bright lines (labeled 2 and 3) run along the image plane, indicating the upper and lower surfaces of the delamination crack which grows from right to left. It can be seen that the delamination does not propagate in a straight line but in a curve along the tow/resin boundary. At the frontier of the delamination indicated by the white square, the two bright lines finally migrate into one. Fig. 3(b) displays a corresponding A-scan signal across the middle of the square in Fig. 3(a). It can be seen that multiple reflections occur at the frontier of the delamination. These could be the reflections from the bridging fibers in-between the crack. Due to the larger refractive index difference between air and composite, the light reflectivity from the crack surface is higher than the one from the fiber and resin interfaces. That explains why in Fig 3(b) the axial signal from the crack area is stronger than the one from other normal area of the specimen, and the delamination crack is more visible than the fiber tows in Fig 3(a).

Therefore, the delamination tip can be observed at the end the crack line, as shown in Fig. 3(c). The exact position of the crack tip can be determined by comparing each axial signal level around the crack region with a threshold decided by the normal signal level from the specimen. The crack length decided in this way should be more accurate than visual decision used in the typical delamination research.

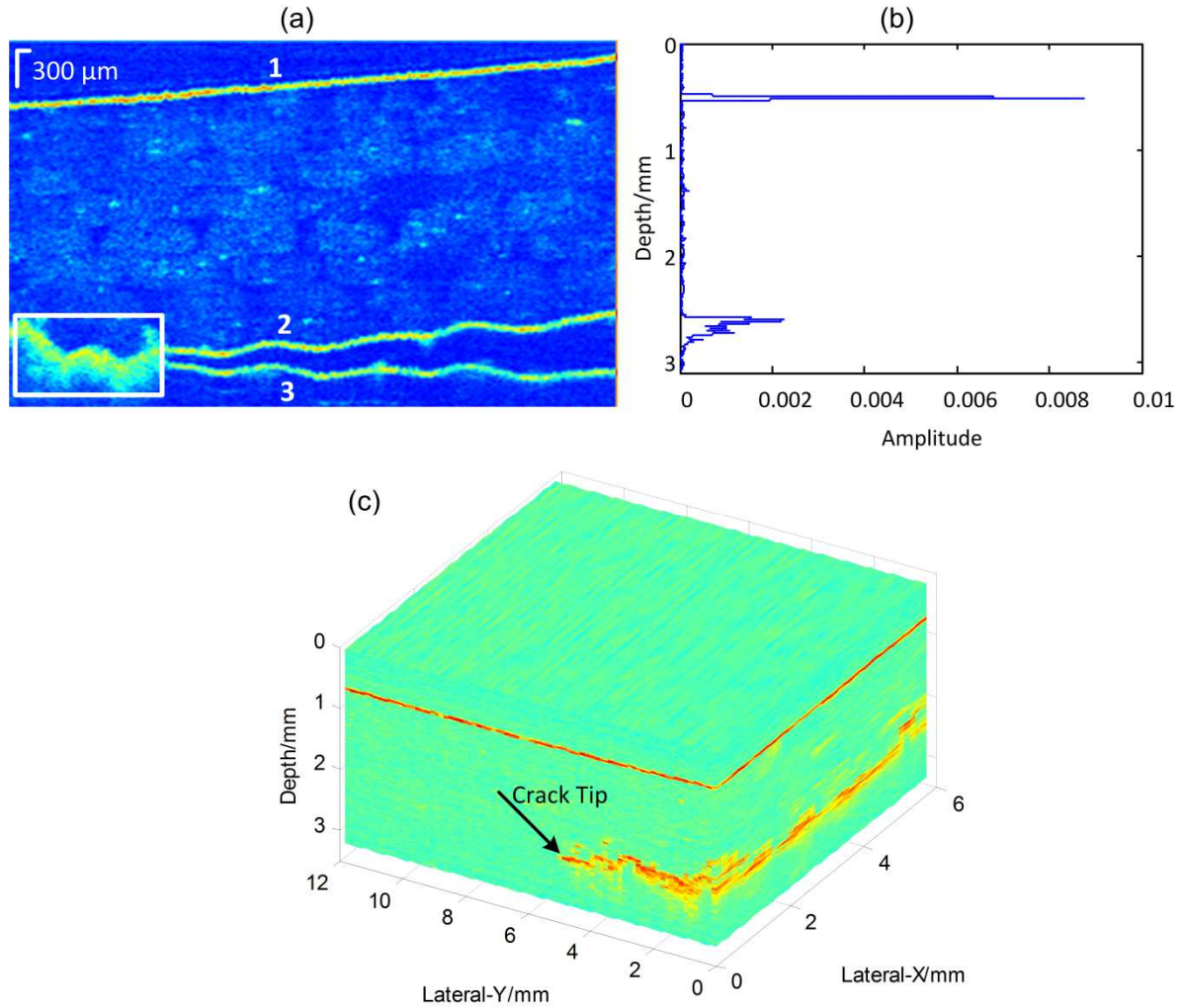


Fig. 3. OCT images from a static test of a delaminated glass fiber composite. (a) A cross-sectional image along the propagation of the delamination. The first bright line indicates specimen surface location, while the second and third bright lines indicate reflections from upper and lower surfaces of the crack. The white square indicates the frontier of the delamination crack. (b) is one depth scan signal across the middle of the white square in (a). (c) is a volumetric image from which crack tip can be observed.

Fig. 3(c) could be a good reference to observe the delamination growth. However a more interesting demonstration is able to observe the crack directly from the front view, which can provide substantial information for delamination research. As shown in Fig. 3(b), multiple reflections occur at the frontier of the delamination. However the first and highest signal peak at this region can be identified as the reflection from the material and crack interface. Therefore the crack surface can be located by peak detection in this region. By 3D OCT scanning in the specimen and further image processing [15], 3D crack surface profiles can be reconstructed, as shown in Fig. 4.

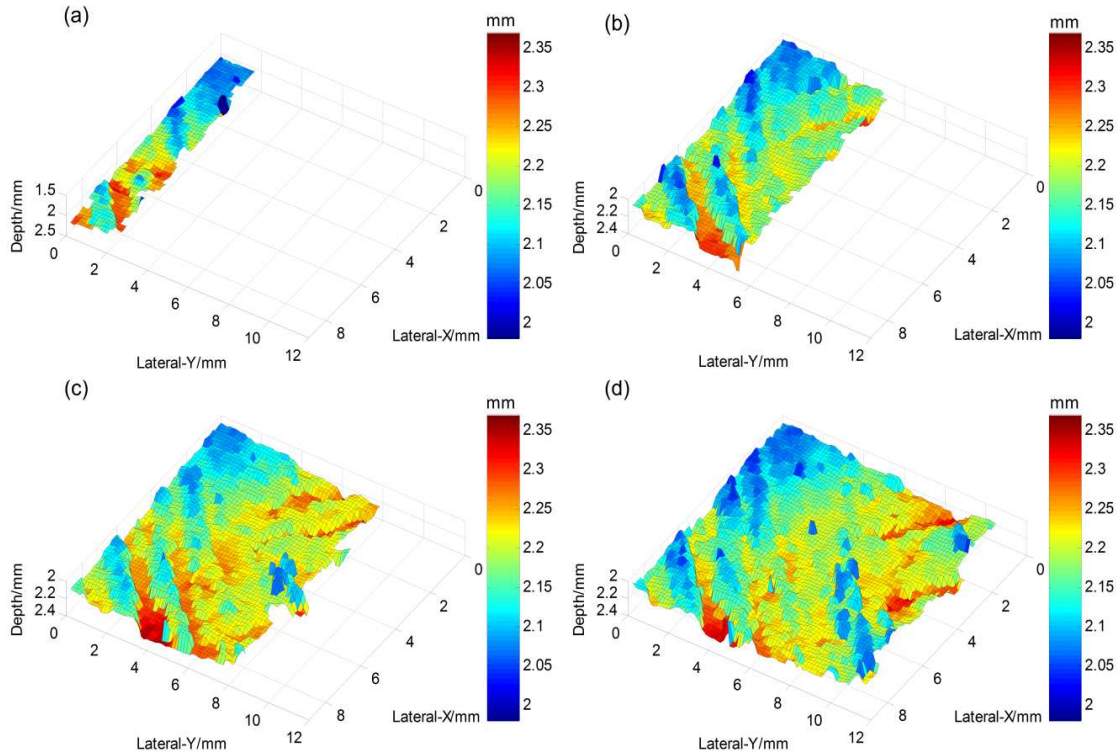


Fig. 4. 3D crack profiles of a glass fiber composite in four stages of delamination growth. The $\pm 45^\circ$ color lines indicate the fiber orientation. The colorbars indicate the surface height.

These crack surface profiles in Fig. 4 were imaged and reconstructed during four stages of delamination growth. It can be seen from the lateral Y scale that the crack lengths at the four stages are 2 mm, 5 mm, 8 mm, and 11 mm respectively. Fig. 4 also clearly shows that the tip of the crack is not in a vertical plane, which indicates the speed of the propagation at different locations is not the same. Moreover, the behavior of crack growth under static loading can be determined. Firstly within a 0 to 3 mm crack length, the delamination crack propagated in a -45° fiber layer. This can be revealed by the -45° lines with blue color. Afterwards the crack at the lower part of the specimen went to the $+45^\circ$ layer underneath the -45° one. This can be revealed by the $+45^\circ$ lines with red color. It is probable that the crack propagated from one layer to a neighboring one, which is usually referred to as a crack jump [16]. Similar results [14] came out from a parallel study of structural nonlinearity at TU Delft on the same specimen type. Both show that the crack can easily propagate into another layer under monotonic and fatigue loadings. The crack jump is one of the most common failure modes recorded when testing multidirectional DCB specimens. Recent studies [17, 18] suggest that crack jump is mainly decided by the bending stiffness of the crack beam and it can be prevented by optimizing the stacking sequence of the fiber layers, which is proved in the next section.

3.2 Carbon Fiber Composites

The composite laminates were produced by hand-lay-up of 32 layers of unidirectional carbon/epoxy prepreg M30SC/DT120 (high strength and modulus carbon fibre/toughened thermosetting epoxy). The layup sequences were designed as $[(0^\circ)_{16} // (0^\circ)_{16}]$ and $[(\pm 45^\circ / (0^\circ)_{12} / \mp 45^\circ) // (\pm 45^\circ / (0^\circ)_{12} / \mp 45^\circ)]$, with consideration of avoiding crack jumping and minimizing both residual thermal stress and non-uniform energy release rate distribution across the width of the crack front [19, 20]. During the manufacturing process, a Teflon film was placed in the middle plane of the composite laminates to act as an initial delamination.

After curing in an autoclave, the composite panels were cut into 200 mm length by 25 width beams. All tests were performed under displacement control with an applied displacement rate of 1 mm/min.

A cross-sectional image and one A-scan signal from one of the delaminated carbon fiber composites are shown in Fig. 5, where the difference from images of a glass fiber composite shown in Fig. 4 can immediately be observed. Due to the opaque carbon fibers, light has difficulty in penetrating the composite specimen and is partly backreflected from the surface, indicated by the bright line in Fig. 5(a) and the peak signal in Fig. 5(b). With OCT it is therefore impossible to monitor the internal delamination growth in carbon fiber composites. Nevertheless, it can still work as a surface profilometer when the composite laminate is finally split into two halves and the crack surfaces are exposed to the OCT probe. Based on the reflection signal from the crack surface, 3D crack profiles can be reconstructed in the same way as performed for glass fiber composite in the previous section.

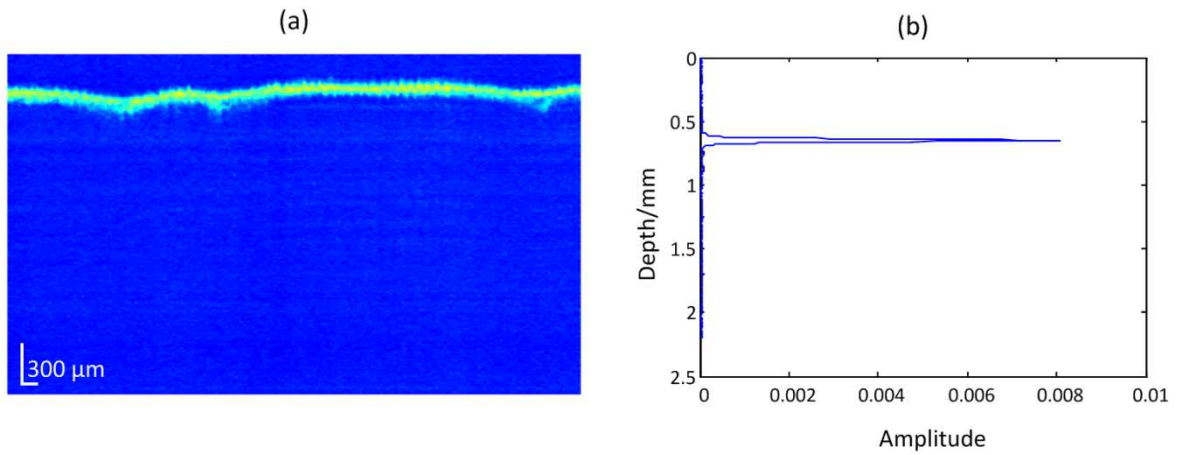


Fig. 5. OCT images from a static test on a delaminated carbon fiber composite. (a) A cross-sectional image along the propagation of the delamination. The first and only bright line indicates specimen surface location, while the subsurface crack is invisible. (b) is one depth scan signal in (a).

Fig. 6(a) and (b) demonstrates the crack surface profiles for $0^\circ//0^\circ$ and $+45^\circ//+45^\circ$ interfaces from two carbon fiber composites respectively. The morphologies of the crack surfaces are significantly different. For delamination growth in the $0^\circ//0^\circ$ interface, the surface is relatively flat, within $\pm 80 \mu\text{m}$ roughness. This indicates delamination growth is constrained in the pre-cracked middle plane because of the fibre orientation in the 0° layer is parallel to the crack growth direction. The fracture surface is much rougher in the $+45^\circ//+45^\circ$ interface, as shown in Fig. 6(b). A typical feature, *peaks and valleys*, all of which are in $+45^\circ$, is observed. This indicates the crack growth in $+45^\circ//+45^\circ$ interface would offset from the pre-cracked middle plane and propagate into the adjacent $+45^\circ$ layer until it reaches the $+45^\circ// -45^\circ$ interface. Due to the fibre constraint in the -45° layer, crack growth cannot jump into the -45° layer and would propagate back into the $+45^\circ$ layer until it reaches another $+45^\circ// -45^\circ$ interface. This pattern would repeat in the delamination growth, leading to a wavelike micro-structure. These 3D crack profiles have proved the success of layup design to avoid the crack jump.

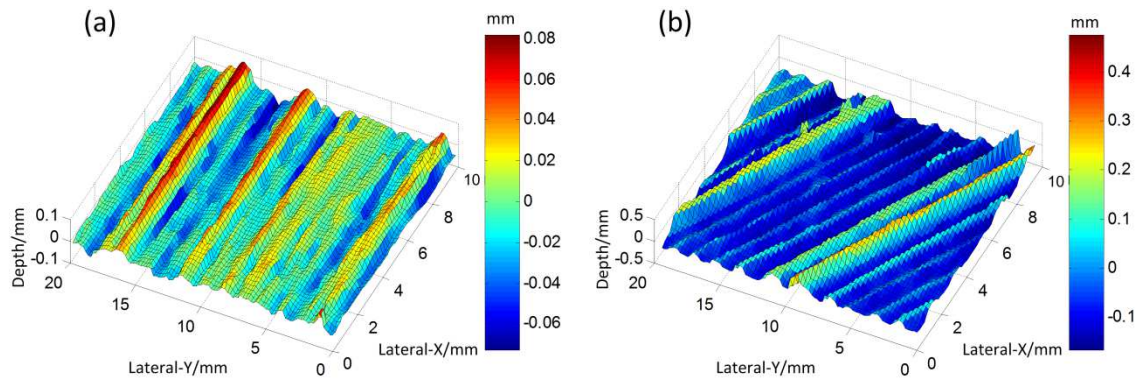


Fig. 6. 3D crack profiles of carbon fiber composites. The 0° and 45° color lines indicate the fiber orientation. The colorbars indicate the surface height.

5. Conclusions

This paper demonstrates the potential advantages of using optical coherence tomography for the study of delamination growth in glass fiber and carbon fiber composites. The customized OCT system can perform as an inline inspection tool to monitor the crack growth and reconstruct the crack surfaces in glass fiber composites. It can also work as a profilometer which is able to rebuild 3D crack profiles within carbon fiber composites. These types of information provided by OCT can let researchers easily access to delamination related parameters, e.g. crack lengths during a tensile test, and observe delamination propagation modes, e.g. crack jump in different layup composites. OCT can greatly improve the facilities for delamination research and could contribute more in the near future with its development in faster and deeper scanning.

References

- [1] W. Cantwell, and J. Morton, "The significance of damage and defects and their detection in composite materials: a review," *The Journal of Strain Analysis for Engineering Design*, 27(1), 29-42 (1992).
- [2] L. Yao, R. Alderliesten, and R. Benedictus, "Interpreting the stress ratio effect on delamination growth in composite laminates using the concept of fatigue fracture toughness," *Composites Part A: Applied Science and Manufacturing*, (2015).
- [3] A. F. Fercher, "Optical coherence tomography," *Journal of Biomedical Optics*, 1(2), 157-173 (1996).
- [4] D. Huang, E. Swanson, C. Lin *et al.*, "Optical coherence tomography," *Science*, 254(5035), 1178-1181 (1991).
- [5] D. Stifter, "Beyond biomedicine: a review of alternative applications and developments for optical coherence tomography," *Applied Physics B*, 88(3), 337-357 (2007).
- [6] A. Nemeth, G. Hanneschlager, E. Leiss *et al.*, [Optical coherence tomography – applications in non-destructive testing and evaluation], Intech (2013).
- [7] D. Stifter, "Nondestructive Material Testing Using OCT," *Optical Coherence Tomography: Technology and Applications*, 2497-2527 (2015).
- [8] M. Wojtkowski, "High-speed optical coherence tomography: basics and applications," *Applied Optics*, 49(16), D30-D61 (2010).
- [9] P. Targowski, M. Góra, and M. Wojtkowski, "Optical coherence tomography for artwork diagnostics," *Laser Chemistry*, 2006, 1-11 (2006).
- [10] P. Liu, [Optical Coherence Tomography for Material Characterization], TU Delft, Delft University of Technology (2014).
- [11] D. Stifter, K. Wiesauer, M. Wurm *et al.*, "Investigation of polymer and polymer/fibre composite materials with optical coherence tomography," *Measurement Science and Technology*, 19(7), 074011 (2008).
- [12] B. E. Bouma, and G. J. Tearney, [Handbook of optical coherence tomography], Marcel Dekker (2002).

- [13] P. Liu, R. M. Groves, and R. Benedictus, "Optical Coherence Tomography for the Study of Polymer and Polymer Matrix Composites," *Strain*, 50(5), 436-443 (2014).
- [14] V. Sridhar, [Combined Numerical & Experimental Methodology for the Detection of Structural Nonlinearity in Composite Wind Turbine Blades], Delft University of Technology (2012).
- [15] P. Liu, R. M. Groves, and R. Benedictus, "3D monitoring of delamination growth in a wind turbine blade composite using optical coherence tomography," *NDT & E International*, 64, 52-58 (2014).
- [16] J. Schön, T. Nyman, A. Blom *et al.*, "A numerical and experimental investigation of delamination behaviour in the DCB specimen," *Composites Science and Technology*, 60(2), 173-184 (2000).
- [17] T. Sebaey, N. Blanco, C. Lopes *et al.*, "Numerical investigation to prevent crack jumping in Double Cantilever Beam tests of multidirectional composite laminates," *Composites Science and Technology*, 71(13), 1587-1592 (2011).
- [18] T. Sebaey, N. Blanco, J. Costa *et al.*, "Characterization of crack propagation in mode I delamination of multidirectional CFRP laminates," *Composites Science and Technology*, 72(11), 1251-1256 (2012).
- [19] L. Yao, R. Alderliesten, M. Zhao *et al.*, "Bridging effect on mode I fatigue delamination behavior in composite laminates," *Composites Part A: Applied Science and Manufacturing*, 63, 103-109 (2014).
- [20] L. Yao, R. Alderliesten, M. Zhao *et al.*, "Discussion on the use of the strain energy release rate for fatigue delamination characterization," *Composites Part A: Applied Science and Manufacturing*, 66, 65-72 (2014).